FIELD EMISSION INVESTIGATION OF CENTRIFUGAL-BARREL-POLISHED Nb SAMPLES

S. Lagotzky*, G. Müller, University of Wuppertal, D-42097 Wuppertal, Germany
A. Navitski, DESY, D-22603 Hamburg, Germany
A. Prudnikava, Y. Tamashevich, University of Hamburg, D-20148 Hamburg, Germany

Abstract

Centrifugal barrel polishing (CBP) of superconducting Nb cavities is recently reconsidered as alternative or complementary to buffered chemical polishing (BCP) and electropolishing (EP). First investigations of the enhanced field emission (EFE) on a Nb sample, which received CBP in a special coupon cavity, were performed. Despite of the rather smooth surface and dry ice cleaning (DIC), EFE already occurred at activation fields E_{act} of 60 MV/m resulting in low onset fields E_{on} of 40 MV/m. This is caused by Al_2O_3 inclusions from the polishing media, which can be removed by 20 µm BCP. Thereby, EFE is shifted to much higher E_{act} of more than 175 MV/m and E_{on} more than 80 MV/m, where EFE is caused by hole-like features with still somewhat sharp edges.

INTRODUCTION

Actual and future linear electron accelerators require high accelerating gradients E_{acc} and quality factors Q_0, which are often limited by enhanced field emission (EFE) in the superconducting Nb cavities [1]. Systematic measurements on Nb samples have revealed particulate contaminations and surface defects as the main origin of EFE [2]. Various elaborate surface preparation (buffered chemical polishing (BCP) and electropolishing (EP)) and cleaning (high-pressure ultra-pure water rinsing (HPR)) techniques are actually used to remove such emitters and obtain a sufficient surface quality. Recently, centrifugal barrel polishing (CBP) has been reconsidered to achieve a smooth surface as after EP but with less effort [3]. Moreover, CBP has been recognized to remove the surface defects like deep scratches, welding splatters, and foreign inclusions, some of which remain unaffected by the EP/BCP. A combination of CBP and EP/BCP was already applied and tested on single-cell Nb cavities with resulting Q_0 of more than 10^{10} and E_{acc} of 25 to 40 MV/m [4-5]. Accordingly, a similar polishing is also considered for the accelerating structures of the future International Linear Collider (ILC) as alternative for the established EP procedure [6-7]. A systematic investigation of the EFE from such CBP surfaces, however, is still pending. Therefore, we have started to investigate the surface quality, EFE statistics and local properties of a Nb sample, which was prepared as a coupon in a modified single-cell 1.3 GHz cavity close to the electric peak field region by an optimized four step CBP process. Instead of HPR, dry ice cleaning (DIC) [8] was used before and after BCP of 20 µm to avoid any particulate emitters.

EXPERIMENTAL DETAILS

Sample Preparation

We have used a polycrystalline Nb disc (Ø of 8.6 mm, thickness of 3 mm, and RRR of 300) with a central thread and small off-axis hole (Ø of 1 mm), which serves for the fixation on a suitable holder during CBP in the cavity. The thread is compatible with the sample holder for the different measurement techniques, while the hole enables a sample repositioning with an accuracy of ~500 µm. The coupon position close to the iris of the modified cavity can be seen in Fig. 1. The CBP was performed in 4 steps with different mixtures of polishing media [9]:

1. Ceramic angle-cut triangles (KM, 9 x 9 mm^2), surfactant (TS compound), and de-ionized (DI) water (8 h, removal rate 3 to 9 µm/h);
2. Plastic cones (RG-22, 12.5 mm), TS compound, and DI water (15 h, removal rate 1 to 2.5 µm/h);
3. 600 mesh Al_2O_3, cubic hardwood blocks (5 mm), and DI water (30 h, removal rate 0.1 to 0.7 µm/h);
4. Colloidal SiO_2 (40 nm) and cubic hardwood blocks (5 mm) (40 h, removal rate less than 0.1 µm/h).

After the CBP, the coupon cavity was rinsed by DI water and cleaned in an ultrasonic bath first with a solvent (TICKOPUR R-33) and then in pure DI water. The CBP sample has received additional DI water rinsing, drying, and protection by a Teflon cap in a clean room.

Finally, CBP sample and Teflon cap were cleaned by DIC with a commercial system (CryoSnow SJ-10) in a cleanroom class ISO 2 for 5 and 3 min, respectively. The

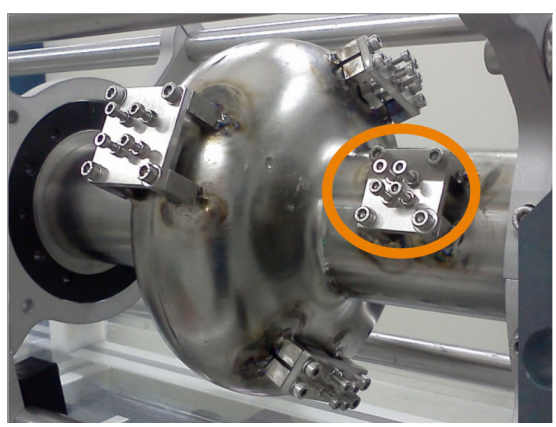

Figure 1: Coupon cavity for the CBP of Nb samples. The circle marks the location of the investigated sample.

*s.lagotzky@uni-wuppertal.de

ISBN 978-3-95450-178-6

protection cap was not removed until the sample faced at least high-vacuum conditions (10^{-5} Pa) and also used during the transport to other measurement systems. Before the second EFE investigation, the sample received a BCP with a polishing depth of 20 μm in a mixture of HF (40%), HNO_3 (65%), and H_3PO_4 (85%) in a ratio of 1:1:2 and again final DIC.

Measurement Techniques

The surface quality of the sample after pure CBP and additional BCP was thoroughly investigated with several techniques. At first, scanning electron microscopy (SEM, Philips PSEM 500) with energy dispersive x-ray analysis (EDX, Bruker AXS, XFlash Detector 5010) and 3D optical microscopy (Keyence VK-X100K) were systematically applied to control the successive removal of surface defects and to reveal possible remnants of the CBP process [9]. In addition, an optical profilometer (OP, FRT MicroProf®) was used, which is installed on a granite plate with an active damping system in a clean (ISO 5) laminar air flow. This OP is based on the spectral reflection and chromatic aberration of white light and provides 3D profiles with less lateral (2 µm) but higher vertical resolution (3 nm). Based on these OP profiles the average R_a and root mean square R_q surface roughness were calculated over selected areas.

For the systematic EFE measurements we have used a non-commercial ultra-high vacuum (10^{-7} Pa) field emission scanning microscope (FESM) [10], which is shown schematically in Fig. 2. The CBP sample was measured in a central area of 3×3 mm^2 after a surface tilt correction relative to the truncated cone anode in order to achieve a constant gap Δz within ±2 µm. The anodes were manufactured from tungsten rods and had a diameter of 100 (300) µm for the investigation of the sample after CBP (CBP/BCP) polishing steps. The FESM employs a PID-regulated power supply (FUG HCN100M-10000, 10 kV, 10 mA) controlled by the EFE current as measured with an analog electrometer (Keithley 610C). Non-destructive voltage scans $V(x,y)$ for a limited EFE current (I_{FE} up to 1 nA) were performed with a resolution of 50 (150) µm before (after) the BCP to localize emitters and to determine the emitter number density N as function of the applied activation field E_{act} in reasonable steps

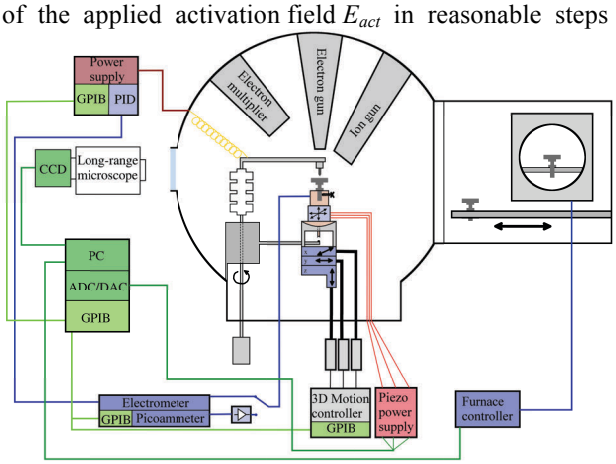

Figure 2: Schematic view of the FESM.

(ΔV of 1 kV). In order to obtain the electric field maps, average Δz values of 40 µm (50 µm) above (below) 200 MV/m were determined by long-range optical microscope images. Due to a slight tilting of the anode (e.g. in the holder or because of manufacturing), the determined values for E_{act} may have an error of up to 10% (30%) for the 100 (300) µm anodes, although in the most cases the error is much lower.

For most of the strong emitters, $I(V)$ characteristics were individually measured up to I_{FE} of 1 nA with a digital picoammeter (Keithley 6485). The actual Δz and thus the local field E were calibrated for each emitter from a PID-regulated $V(z)$ plot for I_{FE} of 1 nA, which also yields the corresponding onset field E_{on} [10]. Using the modified Fowler-Nordheim (FN) law [11]:

$$I_{FE} = A\frac{S\beta^2E^2}{\phi\, t^2(y)}\exp\left(-B\frac{\phi^{3/2}v(y)}{\beta E}\right) \quad (1)$$

the field enhancement factor β and the emitting area S were derived for a given work function φ. For simplicity, we have taken φ = 4 eV, $v(y)$ = $t(y)$ = 1, A = 154 and B = 6830 for E in MV/m and I_{FE} in A. Finally, SEM/EDX (Philips XL30S) analysis of the selected emission sites was used to search for the EFE origin.

RESULTS AND DISCUSSION

Surface Quality

The survey profile of the CBP sample in Fig. 3a shows the off-axis position of the hole with rather sharp edges in comparison to the asymmetrically rounded disc edge. The flatness of the sample is suitable for EFE measurements within a central area of 3×3 mm^2. In addition, five high-resolution scans were performed before and after the BCP, each over an area of 1×1 mm^2 (e.g. Fig. 4). These result in a CBP surface roughness R_a of 130 nm and R_q of 180 nm (cf. Fig. 3b). For comparison, after additional BCP the roughness was drastically increased to R_a of 560 nm and R_q of 730 nm, and the peak-to-peak values increased from ±0.8 to ±3.0 µm. Two large hole-like surface defects were reproducibly found. The dimensions of the one in Fig. 4 were enlarged by BCP from the initial size of ~40 to 70 µm and depth from 6 to 10 µm. The edge of this defect was about 2 µm higher than the surrounding surface before and after the BCP. The dimensions of the second

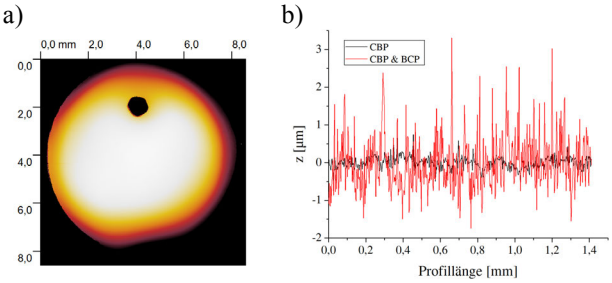

Figure 3: OP map of the full CBP sample (a, area 8.6×8.6 mm^2, lateral resolution 17 µm, height range 200 µm) and selected line profiles before and after BCP (b).

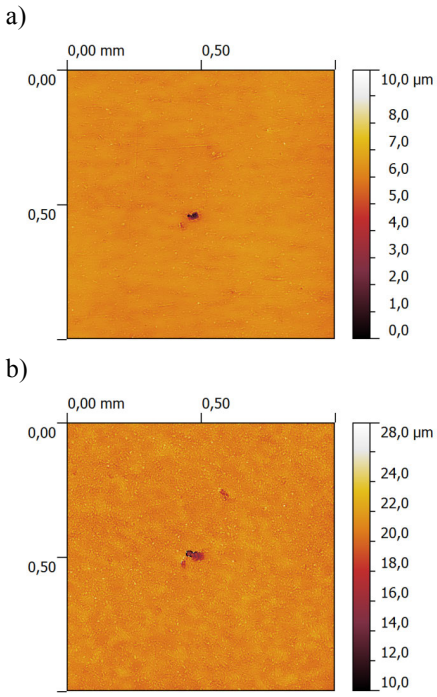

Figure 4: Height maps (1×1 mm^2, 2 µm lateral resolution) of the same surface defect on the CBP sample before (a) and after 20 µm BCP (b).

defect were 20 µm in size, 6 µm in depth and 6 µm in height before and 24, 5, and 6 µm after the BCP, respectively. The OP resolution, however, was not sufficient to determine the curvature radius of these edges for any estimation of the geometrical field enhancement.

In Fig. 5 typical optical microscope images of the CBP sample before and after BCP are compared. Few grooves on the fairly smooth CBP surface are visible, which are most likely created by the impact of the polishing solids. After BCP the surface contains many small defects, which might lead to geometrical field enhancement. Typical SEM images of the pure CBP surface (Fig. 6a) show many insulating inclusions (~10^6 cm^{-2}) with a size of up to 20 µm and sharp rims around them. These inclusions seem to be removed after BCP (Fig. 6b), but many hole-like surface defects with sharp edges appear now. EDX investigations of the surface before and after BCP (Fig. 7) reveal, that the inclusions contain Al. Therefore, these defects are most likely Al_2O_3 particles that are used during the third step of CBP. The removal of these inclusions during BCP causes the hole-like defects.

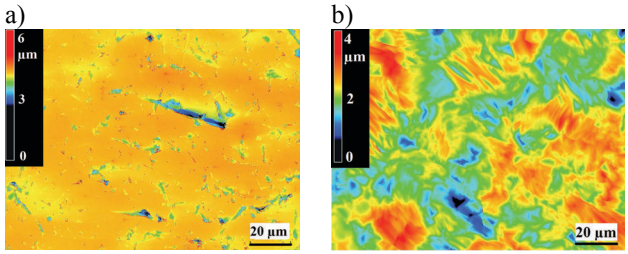

Figure 5: Optical microscope image of the CBP sample before (a) and after BCP (b).

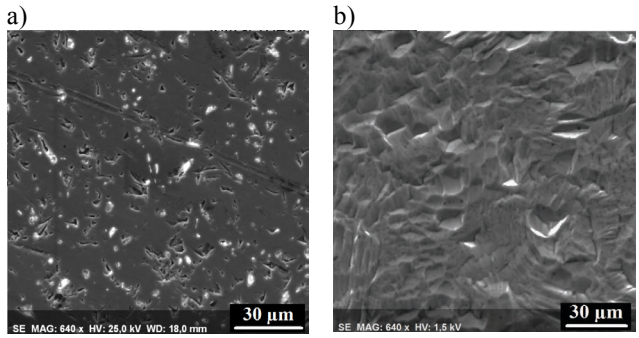

Figure 6: SEM survey image of the CBP sample before (a) and after BCP (b).

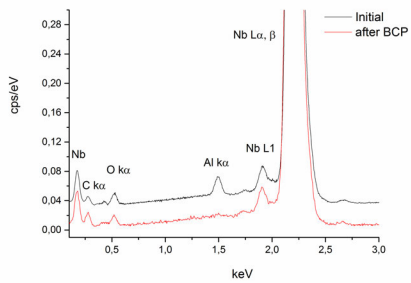

Figure 7: EDX spectra of the CBP sample before and after BCP.

EFE Statistics

The first stable emitter on the CBP surface was already activated at E_{act} of 60 MV/m (Fig. 8a). A strong increase of the emitter number density N with the applied field was observed up to E_{act} of 110 MV/m (Fig. 8b) resulting in N of 128±23 cm^{-2}. After the BCP, however, the first emitter was activated at a rather high E_{act} of 175 MV/m (Fig. 8c) and N increased to 40±13 cm^{-2} at E_{act} of 225 MV/m (Fig. 8d). Accordingly, the EFE was significantly reduced by

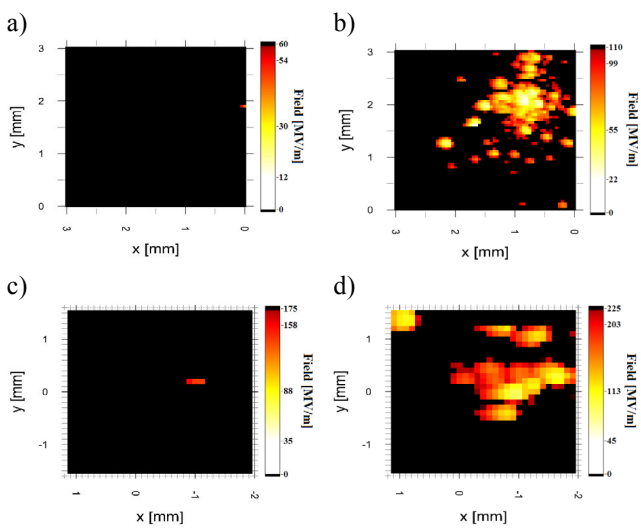

Figure 8: Field maps in the central area of 3×3 mm^2 of the CBP sample with first stable emitter (a, c) and with a high number resolvable emitters (b, c) before (a, b) and after BCP (c, d).

ISBN 978-3-95450-178-6

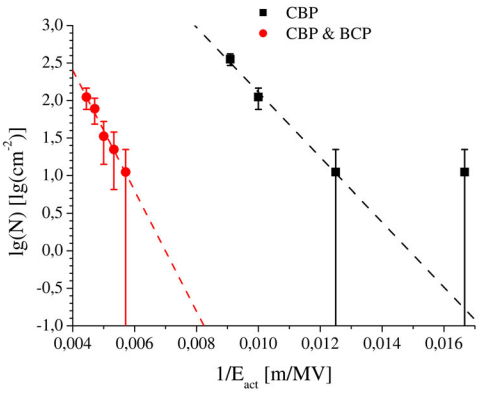

Figure 9: Dependence of the emitter number density from the activation field on the CBP sample before and after 20 µm BCP (plotted in accordance to eq. (2)).

BCP despite of the rougher surface. Furthermore, all field maps showed an activation effect of emitters with significantly decreased onset fields E_{on} compared to their activation field.

In Fig. 9 the resulting $N(E_{act})$ are plotted in accordance to the statstical model for the activation of emitters on metallic surfaces [12]:

$$N(E_{act}) = N_{tot} \cdot \exp(c_s) \cdot \exp\left(-c_s \cdot \frac{E_{\lim}}{E_{act}}\right), \qquad (2)$$

which depends on the total number of potential emitters N_{tot}, the field strength of the native insulating oxide E_{lim}, and surface condition parameter c_s. The linear least-square fit of the data for the CBP surface result in a slope B of -432.68±33 and an y-intercept A of 6.43±0.4. After the BCP, B of -802.63±57 and A of 5.61±0.29 were obtained. The correlation coefficient was rather high (> 0.99) in both cases. Fig. 9 demonstrates the positive effect of the light BCP after the CBP on the EFE at all field levels. Extrapolation of the data to the intended electric peak field of the ILC (E_{peak} = 70 MV/m) results in a drastic reduction of N from 1.8 cm^{-2} to 1.4×10^{-6} cm^{-2}, which would be sufficient for future accelerating structures.

Single Emitter Properties

Guided by the field maps, local EFE measurements and SEM/EDX analysis were performed on 12 (8) strong emission sites before (after) the BCP. For the CBP

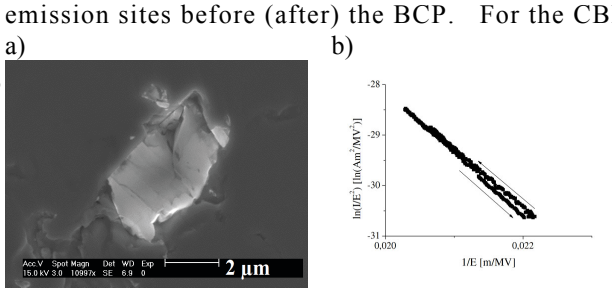

Figure 10: SEM image of an Al_2O_3 inclusion on the CBP surface (a) and corresponding FN plot (b, see eq. 1) with β of 47, S of 11 µm^2, and E_{on} of 47.8 MV/m (b).

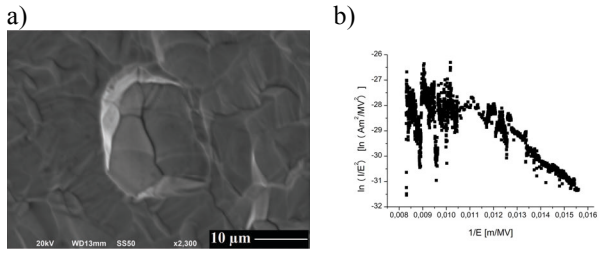

Figure 11: SEM image of a typical emission site after the BCP (a) and corresponding FN plot (b, see eq. 1) with β of 15, S of 6.4×10^{-3} µm^2, and E_{on} of 188.9 MV/m (b).

surface the EFE was mainly caused by Al_2O_3 inclusions, which stem from the third step of the CBP process. Therefore, triple junctions are created between the Nb/Al_2O_3 interface and the vacuum, which are known as strong emitters [13]. Fig. 10 shows a typical example that caused strong stable EFE. After the BCP, these inclusions were completely removed, but hole-like features with still somewhat sharp edges were always found in the emission regions (Fig. 11). This EFE, however, was significantly weaker, less stable, and not correlated to the base roughness.

The obtained E_{on} range of the emitters was significantly increased by the BCP from 40 to 120 MV/m range in the case of CBP polished surface to 80 to 180 MV/m range for the surface with the additional 20 µm BCP polishing (Fig. 12a). The shift of E_{on} is mainly caused by a decrease

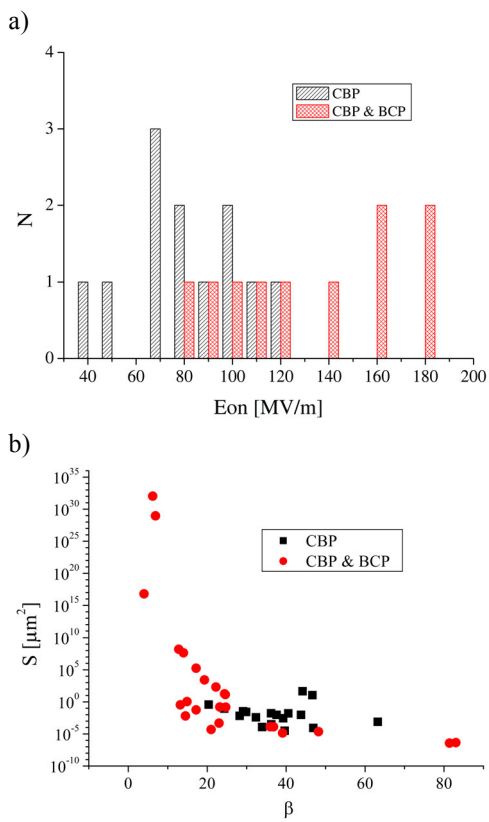

Figure 12: Distribution of the E_{on} field of emitters (a) and correlation of FN-parameters S and β (b) before and after the additional BCP.

of β after the BCP (Fig. 12b), which can be explained by the less sharp edges of the hole-like features. Furthermore, some emission sites showed a current switching resulting in unreasonably high S values with respect to the anode size. These are most likely caused by resonant tunnelling effects, which only appear after the BCP. Therefore, always present surface adsorbates [14] seem to be less harmful for EFE than Nb oxides [15], which might depend on the polishing technique. It is most remarkable that the finally achieved E_{on} values are higher than E_{peak} of the ILC cavities.

CONCLUSIONS AND OUTLOOK

The surface of CBP-polished niobium is rather smooth in terms of average roughness but contains many Al_2O_3 inclusions and sharp rims around them due to the mechanical polishing process. Despite of DIC cleaning, these cause strong EFE activation at E_{act} field starting from 60 MV/m and onset field E_{on} starting from 40 MV/m probably due to triple junctions. After additional 20 µm BCP, however, such inclusions and sharp rims are removed and EFE is shifted to much higher field values (E_{act} more than 175 MV/m and E_{on} more than 80 MV/m), despite of an increased surface roughness. The remaining less-stable EFE is caused by hole-like features with less-sharp edges and lead sometimes to unreasonably high S-values, what hints for resonant tunnelling by oxides. It is most remarkable, that a combination of CBP, BCP, and DIC enables an EFE suppression of polycrystalline Nb up to field values above the intended electric peak-fields of future ILC cavities.

As next step, the CBP process should be optimized to reduce the damage layer and amount of the inclusions and thus the required BCP depth. Alternatively, a light EP instead of the BCP might help to suppress EFE more effectively.

ACKNOWLEDGMENT

The work was funded by BMBF project 05H12PX6.

REFERENCES

[1] D. Reschke, S. Aderhold, et al., THPP021, Proc. LINAC14, http://jacow.org.
[2] A. Navitski, S. Lagotzky et al., Phys. Rev. ST – Accel. Beams **16**, 112001 (2013).
[3] C. A. Cooper, L. D. Cooley, Supercond. Sci. Technol. **26**, 015011 (2013).
[4] T. Higuchi, T. Suzuki, et al., SRF95F34, Proc. SRF95, http://jacow.org.
[5] G. Issarovitch, D. Proch, et al., TUP56, Proc. SRF03, http://jacow.org.
[6] C. Cooper, J. Brandt, et al., THPPO076, Proc. SRF09, http://jacow.org.
[7] A. D. Palczewski, C. A. Cooper, et al., TUIOB01, Proc. SRF13, http://jacow.org.
[8] S. Lagotzky, P. Serbun, et al., WEPME005, Proc. IPAC14, http://jacow.org.
[9] A. Navitski, E. Elsen, B. Foster, A. Pudnikava, Y. Tamashevich, "Surface analyses and optimization of centrifugal barrel polishing of Nb cavities", MOPB073, this conference.
[10] D. Lysenkov, G. Müller, Int. J. Nanotechnol. **2**, 239 (2005).
[11] R. G. Forbes, J. Vac. Sci. Technol. B **17**, 526 (1999).
[12] S. Lagotzky, G. Müller, submitted to Nucl. Instr. Methods Phys. Res. Sect. A (2015).
[13] M. Chhowalla, C. Ducati, et al., Appl. Phys. Lett. **79**, 2079 (2001).
[14] A. Zeitoun-Fakiris and B. Juttner, J. Phys. D: Appl. Phys. **21**, 960 (1988).
[15] J. Halbritter, Surf. Sci. **122**, 80 (1982).

ISBN 978-3-95450-178-6